Topological superconductor in quasi-one-dimensional $Tl_{2-x}Mo_6Se_6$

Shin-Ming Huang, Chuang-Han Hsu, Su-Yang Xu, Chi-Cheng Lee, Shiue-Yuan Shiau, Hsin Lin, and Arun Bansil

Phys. Rev. B **97**, 014510 — Published 16 January 2018

DOI: 10.1103/PhysRevB.97.014510

Topological superconductor in quasi-one-dimensional $Tl_{2-x}Mo_6Se_6$

Shin-Ming Huang,[1] Chuang-Han Hsu,[2,3] Su-Yang Xu,[4]
Chi-Cheng Lee,[5] Shiue-Yuan Shiau,[2,3] Hsin Lin,[2,3,6] and Arun Bansil[7]

[1]*Department of Physics, National Sun Yat-sen University, Kaohsiung 80424, Taiwan*
[2]*Centre for Advanced 2D Materials and Graphene Research Centre, National University of Singapore, 6 Science Drive 2, Singapore 117546*
[3]*Department of Physics, National University of Singapore, 2 Science Drive 3, Singapore 117542*
[4]*Department of Physics, Massachusetts Institute of Technology, Cambridge, Massachusetts 02139, USA*
[5]*Institute for Solid State Physics, The University of Tokyo, Kashiwa 277-8581, Japan*
[6]*Institute of Physics, Academia Sinica, Nankang Taipei 11529, Taiwan*
[7]*Department of Physics, Northeastern University, Boston, Massachusetts 02115, USA*

(Dated: December 28, 2017)

We propose that the quasi-one-dimensional molybdenum selenide compound $Tl_{2-x}Mo_6Se_6$ is a time-reversal-invariant topological superconductor induced by inter-sublattice pairing, even in the absence of spin-orbit coupling (SOC). No noticeable change in superconductivity is observed in Tl-deficient ($0 \leq x \leq 0.1$) compounds. At weak SOC, the superconductor prefers the triplet d vector lying perpendicular to the chain direction and two-dimensional E_{2u} symmetry, which is driven to a nematic order by spontaneous rotation symmetry breaking. The locking energy of the d vector is estimated to be weak and hence the proof of its direction would rely on tunnelling or phase-sensitive measurements.

I. INTRODUCTION

Topological superconductivity stands out among all the topological phases in part because the Majorana fermions it allows at boundaries are not only fundamentally fascinating but also have potential applications in quantum computation[1–5]. A crucial element for such superconductors is spin-triplet pairing, or odd-parity pairing in the presence of inversion symmetry[6,7]. Prime examples are unconventional superconductors Sr_2RuO_4[8,9] and UPt_3[10] and both of them act as chiral superconductors[11–13]. However, their complex or nodal Fermi surface properties make it difficult to host distinct Majorana modes[8,10,13,14]. One could seek to exploit the proximity effect between the surface states of an topological insulator and an s-wave superconductor[3,15–17]. Such a approach requires strong spin-orbit coupling (SOC) to break the inversion symmetry in order to turn singlet pairing into triplet pairing. Another rather unexpected avenue toward realizing topological superconductors is through doping topological insulators. The electron-doped topological insulator $Cu_xBi_2Se_3$ has just been verified as a spin-triplet superconductor with a critical temperature $T_c \sim 3.2$ K[7,18,19], and possibly carrying a nematic order[19–21].

In this Letter, we propose the non-symmorphic semimetal compound $Tl_{2-x}Mo_6Se_6$ as a spin-triplet topological superconductor with time-reversal symmetry. Being a representative of molybdenum selenides $\mathcal{M}_2Mo_6Se_6$ ($\mathcal{M}$=Na, Rb, In, or Tl), this compound becomes superconducting with $T_c \sim 3 - 6.5$ K[22–25], and is fully gapped according to differential resistance studies[26]. Tl deficiency x falls between 0 to 0.1. Another superconductor in the family is $\mathcal{M}$=In compound with $T_c \sim 2.9$ K[25]. $Tl_{2-x}Mo_6Se_6$ superconductor is particularly interesting because a small SOC will suffice to fix the triplet d vector[27] and yield a two-component order parameter in the E_{2u} irreducible representation. Moreover, the superconductivity is rather insensitive to doping within the available experimental doping range ($0 \leq x \leq 0.1$). Similar to $Cu_xBi_2Se_3$ superconductor, we expect a concurrent nematic order[20], and a nematic vortex from the crossing of nematic domain walls, around which (pseudo)spin-up and spin-down order parameters gain phases of $\pm 2\pi$, will bind the Kramers pair of Majorana modes robust against disorder[28].

II. CRYSTAL SYMMETRY AND ELECTRONIC STRUCTURE

Non-symmorphic compound $Tl_{2-x}Mo_6Se_6$ has a hexagonal lattice with inversion symmetry, characterized by the space group $P6_3/m$ (No. 176). Having highly anisotropic lattice constants (a=8.934 $\mathring{A}$, c=4.494 $\mathring{A}$), its crystal structure is quasi-one-dimensional (quasi-1D), with Mo_3Se_3 chains arranged in a triangular lattice, as shown in Figs. 1(a,b). A Tl atom is centered in each triangle to couple the Mo_3Se_3 chains. It also act as an electron donor, stable in a +1 valence state, much like an alkali atom[25]. Two inverse closely-packed Mo_3 triangles at $3\vec{c}/4$ and $\vec{c}/4$, dubbed A and B, form a basis of the Mo_3Se_3 chain. Owing to neighboring three Se anions and one Tl cation, three Mo atoms of a triangle have to share five $4d$ valence electrons, which implies a half-filled band in the absence of Tl deficiency.

We have performed first-principles band calculations[29] within density functional theory using generalized gradient approximation[30]. $Tl_{2-x}Mo_6Se_6$ band structures are shown in Fig. 2. The bands close to the Fermi level mainly come from the Mo d_{xz} orbitals with lobes of their Wannier wave functions pointing toward nearby Se atoms

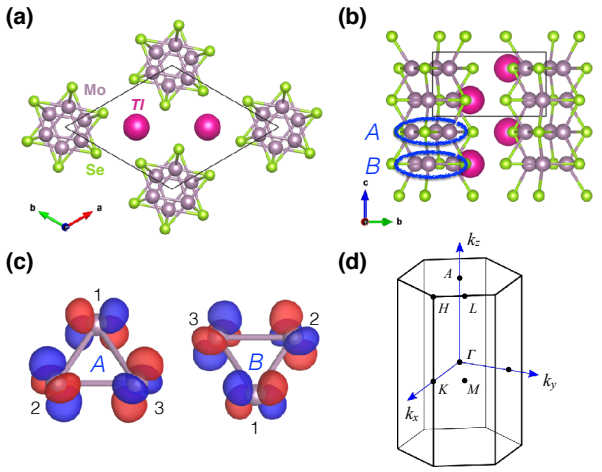

FIG. 1: (Color online) Hexagonal lattice and Brillouin zone of $Tl_2Mo_6Se_6$. (a,b) Top/Side view of a unit cell. Large pink, median purple and small green spheres denote Tl, Mo and Se atoms, respectively. In a unit cell, two Mo triangles, A and B, form the (electronic) basis. (c) Wannier functions for A and B sublattices come from d_{xz} orbitals and are C_3-invariant. Red and blue colors in the Wannier function stand for opposite signs. (d) The first Brillouin zone and high-symmetry k points. Γ, M, A, and L are time-reversal invariant momenta.

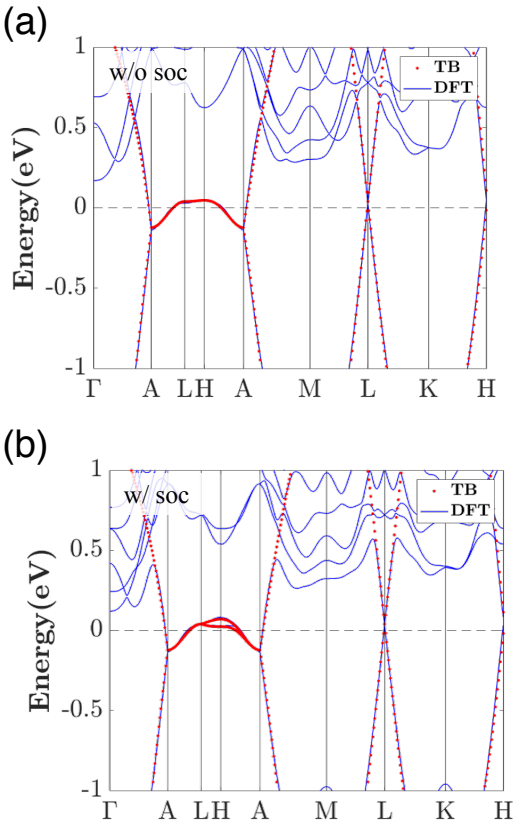

FIG. 2: (Color online) Band structures of undoped $Tl_2Mo_6Se_6$ with (a) or without (b) SOC. Blue lines represent results from first-principles calculations and red dots from fitting the tight-binding model. The Fermi energy is set to zero.

[see Fig. 1(c)]. They are the basis states from which we construct the low-energy Hamiltonians. Two A and B sublattice states can interchange under inversion $\mathcal{I}$, the center of inversion being in the middle of the two sublattices. They can also interchange by a two-fold screw operation $\mathcal{S}_2$ along the z direction, plus a translation by $\vec{c}/2$.

Consider first a simple 1D Mo_3Se_3 chain in the z direction. (Throughout the paper we shall set lattice constants to unity.) The two sublattices in a unit cell form symmetric and anti-symmetric states and they modulate with phase $e^{ik_z z}$ to be a bonding and a anti-bonding band. At $k_z = \pi$, the Bloch-state modulating phase is equal to $(-1)^z$ and the bonding and anti-bonding states become identical under inversion, $\mathcal{I}\Psi_{\rm Bond} = \Psi_{\rm Antibond}$ (up to a phase), so that two bands touch.

By extending to three dimensions through introducing inter-chain coupling, the band crossing evolves into a two-dimensional (2D) nodal surface at $k_z = \pi$[31]. The two-band Hamiltonian reads

$$\mathcal{H}_t(\mathbf{k}) = \varepsilon_0(\mathbf{k})\sigma_0 + \varepsilon_1(\mathbf{k})\sigma_1 + \varepsilon_2(\mathbf{k})\sigma_2, \qquad (1)$$

where σ_0 and σ_i are the identity and Pauli matrices for sublattices. The σ_3 term is forbidden by the $\mathcal{TI}$ symmetry (referred to Appendix A). Furthermore, $(\mathcal{TS}_2)^2$ is a unit lattice translation by $\vec{c}$ and gives e^{-ik_z} by acting on a Bloch eigenstate. Particularly, $(\mathcal{TS}_2)^2 = -1$ at $k_z = \pi$, leading to a double degeneracy for all states, analogous to the Kramers degeneracy[31]. As a result, $\varepsilon_1(\mathbf{k}) = \varepsilon_2(\mathbf{k}) = 0$ at $k_z = \pi$. As shown in Fig. 2(a), states along the A-L-H-A path on $k_z = \pi$ plane are degenerate.

Under time-reversal and inversion symmetries, the Hamiltonian that includes SOC reads, derived in Appendix A,

$$\mathcal{H}(\mathbf{k}) = s_0\mathcal{H}_t(\mathbf{k}) + \vec{\zeta}(\mathbf{k})\cdot\vec{s}\,\sigma_3, \qquad (2)$$

where s_0 and $\vec{s} = (s_1, s_2, s_3)$ are the identity and Pauli matrices for spin. As a consequence of $\mathcal{T}$ and $\mathcal{I}$ symmetries, ζ's must be odd in $\mathbf{k}$. This σ_3 term will gap out the surface node. According to first-principles calculations, the SOC is quite weak for Tl atom, especially along $A-L$, but gets larger for heavier $\mathcal{M}$ atom [see Fig. 2(b)]. Since SOC vanishes at time-reversal invariant momenta, residual point-like band crossings appear at A and L points, namely three-dimensional (3D) Dirac nodes. In particular, the band crossing at A point is a cubic Dirac fermion due to its six-fold symmetry[32].

III. THEORY OF SUPERCONDUCTIVITY

Under time-reversal symmetry, the $Tl_2Mo_6Se_6$ superconducting states, described by the mean-field Hamiltonian

$$\mathcal{H}_{\rm SC}(\mathbf{k}) = \begin{pmatrix} \mathcal{H}(\mathbf{k})-\mu & \Delta(\mathbf{k}) \\ \Delta(\mathbf{k}) & -[\mathcal{H}(\mathbf{k})-\mu] \end{pmatrix} \quad (3)$$

in the basis $\Psi_{\mathbf{k}} = (\psi^{\rm T}_{\mathbf{k}\uparrow}, \psi^{\rm T}_{\mathbf{k}\downarrow}, \psi^{\dagger}_{-\mathbf{k}\downarrow}, -\psi^{\dagger}_{-\mathbf{k}\uparrow})^{\rm T}$, can be classified into even (spin singlet) and odd parity (spin triplet) pairing by $\mathcal{I}\Delta(\mathbf{k})\mathcal{I}^{-1} = \pm\Delta(-\mathbf{k})$. For a DIII topological superconductor, the parity of the superconducting gap has to be odd[6]. In conventional superconductivity, spin singlet/triplet imposes that the gap function is even/odd in $\mathbf{k}$. However, additional sublattice degrees of freedom plays a role much like in the orbital pairing theory in Fe-based superconductors[37]: For spin singlet, to make parity even, we can have sublattice and $\mathbf{k}$ parts to be both even or both odd. For spin triplet, to make parity odd, we can have sublattice even and $\mathbf{k}$ odd, or sublattice odd and $\mathbf{k}$ even. Since $\mathcal{I}$ is a combination of the two-fold screw operation $\mathcal{S}_2$ and mirror operation $\mathcal{M}_z$ (i.e., $z \to -z$), we can further classify the superconducting states in each parity into screw even (+) and screw odd (−), according to

$$\mathcal{S}_2(k_z)\Delta(k_x,k_y,k_z)\mathcal{S}_2(k_z)^{\rm T} = \pm\Delta(-k_x,-k_y,k_z).$$

Similarly for $\mathcal{M}_z$.The full classification of the gap functions according to C_{6h} group is shown in Table I.

We consider attractive, intra- and inter-sublattice interactions for pairing,

$$H_{\rm int} = -\sum_{\mathbf{r}}\Big\{U\big[n_{A\uparrow}(\mathbf{r})n_{A\downarrow}(\mathbf{r}) + n_{B\uparrow}(\mathbf{r})n_{B\downarrow}(\mathbf{r})\big] + V\big[n_A(\mathbf{r})n_B(\mathbf{r}+\vec{c}/2) + n_A(\mathbf{r})n_B(\mathbf{r}-\vec{c}/2)\big]\Big\}, \quad (4)$$

where $\mathbf{r}$ runs over the Bravais lattice and $n_X(\mathbf{r}) = n_{X\uparrow}(\mathbf{r}) + n_{X\downarrow}(\mathbf{r})$ is the electron density for sublattice X. Interactions between chains are neglected since we expect pairing to be the strongest within a chain. Table I lists six possible pairing symmetries. While the intra-sublattice interactions participate in the A_g pairing, the inter-sublattice interactions contribute to all six pairings. Details in Appendix A. Their critical temperatures T_c are determined by

$$\det\left[\begin{pmatrix} \frac{U}{4}\chi_0(T_c) & \frac{U}{4}\chi_{01}(T_c) \\ \frac{V}{2}\chi_{01}(T_c) & \frac{V}{2}\chi_1(T_c) \end{pmatrix} - \mathrm{I}\right] = 0, \quad \text{for} \quad \Delta_1$$
$$\frac{V}{2}\chi_i(T_c) = 1, \quad \text{for} \quad \Delta_{i=2,3,4,5,6}. \quad (5)$$

The pair susceptibility χ_i is given by

$$\chi_i = \frac{T}{N}\sum_{\mathbf{k},i\omega_n} \mathrm{Tr}\big(\Gamma_i(\mathbf{k})G(\mathbf{k},i\omega_n)\Gamma_i(\mathbf{k})G(\mathbf{k},-i\omega_n)\big), \quad (6)$$

where $G(\mathbf{k},i\omega_n) = [i\omega_n - \mathcal{H}(\mathbf{k}) + \mu]^{-1}$ with $\omega_n = (2n+1)\pi k_B T$ is the fermion Green's function, and N is the number of lattice sites. The chemical potential μ is used to simulate doping effect. The vertex functions are $\Gamma_0(\mathbf{k}) = s_0\sigma_0$, $\Gamma_1(\mathbf{k}) = s_0\sigma_1\cos(k_z/2)$, $\Gamma_2(\mathbf{k}) = s_0\sigma_2\sin(k_z/2)$, $\Gamma_3(\mathbf{k}) = s_3\sigma_1\sin(k_z/2)$, $\Gamma_4(\mathbf{k}) = s_3\sigma_2\cos(k_z/2)$, $\Gamma_5(\mathbf{k}) = s_1\sigma_2\cos(k_z/2)$, and $\Gamma_6(\mathbf{k}) = s_1\sigma_1\sin(k_z/2)$. χ_{01} is obtained by replacing the first $\Gamma_i(\mathbf{k})$ in Eq. (6) by $\Gamma_0(\mathbf{k})$ and the second by $\Gamma_1(\mathbf{k})$.

Adopting the fitting parameters for the band structure in Fig. 2(b), we computed the pair susceptibility for these six channels [see Fig. 3(a)]. Three dominant channels are χ_0, χ_3 and χ_6 for, respectively, 1D A_g and A_u, and 2D E_{2u} irreducible representations, all having sublattice-even and screw-even pairings. In Table I, those for gapful superconductivity show the conventional logarithmic behavior, $\chi \sim \mathcal{N}_{\rm eff}\ln(\Lambda/k_{\rm B}T)$, where $\mathcal{N}_{\rm eff}$ stands for the effective density of states at the Fermi energy and Λ is the energy cutoff. The logarithmic law taken into Eq. (5) determines the critical temperature for superconductivity.

We first consider A_g and E_{2u} states. Depending on the interaction strength ratio U/V, the superconductor can fall into A_g or E_{2u} state. From Eq. (5), the condition for E_{2u} to dominate over A_g is

$$\frac{U}{2V} < \frac{\tilde{\chi}_1 - 1}{\tilde{\chi}_0(\tilde{\chi}_1 - 1) - \tilde{\chi}_{01}^2} \quad (7)$$

where $\tilde{\chi}_{0,01,1} = \chi_{0,01,1}(T_c)/\chi_6(T_c)$; otherwise, A_g dominates over E_{2u}. The phase diagram is shown in Fig. 3(b). Doping would only slightly shift the phase boundary and reduce T_c. At present little is known about the origin of pairing and the values of U and V. If the attractive interactions are phonon-mediated, the spin triplet state could be stabilized by a weak electronic correlation, as proposed for $Cu_xBi_2Se_3$[38]. Then, considering that strong on-site repulsion is common in $4d$ transition metals, the E_{2u} state is likely the winner.

The critical temperatures for A_u and E_{2u} states are very close since their χ difference is small (the estimation is found in Appendix B. In the absence of SOC, the E_{2u} state will be triply degenerate with the A_u state because of SU(2) spin symmetry. The SOC lifts their degeneracy, favoring E_{2u}. The solution to the fact is that the highest T_c is obtained when the triplet d vector aligns with the SOC field $\vec{\zeta}(\mathbf{k})$ in Eq. (2)[39]. For the Fermi surface located around $k_z = \pi$, $\vec{\zeta}(\mathbf{k})$ and hence the d vector, in principle lies on the x-y plane.

IV. NEMATIC ORDER

To study spontaneous time-reversal and rotation symmetry breaking, we consider the phenomenological Ginzburg-Landau free energy for the spin-triplet E_{2u}

Rep.	$\mathcal{S}_2$	$\mathcal{M}_z$	Basis functions	$\Delta(\mathbf{k})$	Susceptibilities
A_g (Δ_1)	$+$	$+$	1	$s_0\otimes\sigma_0;\cos\frac{k_z}{2}s_0\otimes\sigma_1$	χ_0,χ_{01},χ_1
B_g (Δ_2)	$-$	$-$	$\mathrm{Re}\,k_+^3k_z;\mathrm{Im}\,k_+^3k_z$	$s_0\otimes\sin\frac{k_z}{2}\sigma_2$	χ_2
E_{1g}	-2	-2	$\left\{\begin{array}{c}k_xk_z\\k_yk_z\end{array}\right\}$	N/A	
E_{2g}	$+2$	$+2$	$\left\{\begin{array}{c}k_x^2-k_y^2\\2k_xk_y\end{array}\right\}$	N/A	
A_u (Δ_3)	$+$	$-$	$k_z\hat{z};k_x\hat{x}+k_y\hat{y};k_x\hat{y}-k_y\hat{x}$	$s_3\otimes\sin\frac{k_z}{2}\sigma_1$	χ_3
B_u (Δ_4)	$-$	$+$	$\mathrm{Re}\,k_+^3\hat{z};\mathrm{Im}\,k_+^3\hat{z}$	$s_3\otimes\cos\frac{k_z}{2}\sigma_2$	χ_4
E_{1u} (Δ_5)	-2	$+2$	$\left\{\begin{array}{c}k_x\hat{z}\\k_y\hat{z}\end{array}\right\};\left\{\begin{array}{c}k_z\hat{x}\\k_z\hat{y}\end{array}\right\}$	$\left\{\begin{array}{c}s_1\\s_2\end{array}\right\}\otimes\cos\frac{k_z}{2}\sigma_2$	χ_5
E_{2u} (Δ_6)	$+2$	-2	$\left\{\begin{array}{c}(k_x^2-k_y^2)k_z\hat{z}\\2k_xk_yk_z\hat{z}\end{array}\right\};\left\{\begin{array}{c}k_x\hat{x}-k_y\hat{y}\\k_y\hat{x}+k_x\hat{y}\end{array}\right\}$	$\left\{\begin{array}{c}s_1\\s_2\end{array}\right\}\otimes\sin\frac{k_z}{2}\sigma_1$	χ_6

TABLE I: Classification of gap functions for the interaction in Eq. (B1) in C_{6h} group. g (u) subscript denotes even (odd) parity. A's and B's are 1D representations, E's are 2D representations. The second and third columns display traces of eigenvalues of $\mathcal{S}_2$ and $\mathcal{M}_z$ for every representation. The gap function is defined by $\Delta(\mathbf{k})=s_i\otimes\sum_{j=0}^{3}\Delta_j(\mathbf{k})\sigma_j$. s_0 stands for spin singlet ($\uparrow\downarrow-\downarrow\uparrow$), and $s_{1,2,3}$ stands for spin triplet ($\uparrow\uparrow-\downarrow\downarrow$, $\uparrow\uparrow+\downarrow\downarrow$, $\uparrow\downarrow+\downarrow\uparrow$), respectively. σ_0 and σ_3 (σ_1 and σ_2) terms are intra- (inter-)sublattice pairings. σ_0 and σ_1 (σ_2 and σ_3) terms are sublattice even (odd). The basis functions allude to gap functions from the band particles (Here k's are expanded around the A point and $k_+=k_x+ik_y$).

state, which reads

$$\begin{aligned}F=&\alpha\left(|\Psi_+|^2+|\Psi_-|^2\right)+\beta_1\left(|\Psi_+|^2+|\Psi_-|^2\right)^2\\&+\beta_2|\Psi_+|^2|\Psi_-|^2,\end{aligned}\tag{8}$$

where $\Psi_\pm=\Psi_1\pm i\Psi_2$. The two order parameters for E_{2u}, Ψ_1 and Ψ_2, correspond to the pairing states $i\langle c_{A\uparrow}^\dagger c_{B\uparrow}^\dagger-c_{A\downarrow}^\dagger c_{B\downarrow}^\dagger\rangle$ and $\langle c_{A\uparrow}^\dagger c_{B\uparrow}^\dagger+c_{A\downarrow}^\dagger c_{B\downarrow}^\dagger\rangle$, respectively. Below T_c ($\alpha<0$), we obtain $\Psi_{1,2}\neq0$ and superconductivity occurs. The sign of β_2 is crucial for determining whether time-reversal symmetry ($\beta_2>0$) or rotation symmetry ($\beta_2<0$) breaks[20]. We shall rule out the $\mathcal{T}$-breaking scenario since no magnetic moment is found in $Tl_{2-x}Mo_6Se_6$[24]. In order to determine the nematic angle θ in the crystal, we need the sixth-order term in the free energy, given by

$$\delta F_6=-(\gamma_1+i\gamma_2)\left(\Psi_+^*\Psi_-\right)^3+\mathrm{H.c.}\tag{9}$$

where (γ_1,γ_2) depend on microscopic models. This term is proportional to $-\sqrt{\gamma_1^2+\gamma_2^2}\cos(6\theta-\phi)$ with $\phi=\arctan(\gamma_2/\gamma_1)$; so, θ is pinned at $\phi/6+2n\pi/3$ with arbitrary integer n. (For a nematic order, θ and $\theta+\pi$ are equivalent.) In contrast to $Cu_xBi_2Se_3$ whose nematic state is possibly nodal[20,40], $Tl_{2-x}Mo_6Se_6$ has a nematic state that is fully gapped for any θ.

Regardless of the nematic angle, a Kramers pair of Majorana flat bands will barbor on the (001) surface, which is guaranteed by a nonzero 1D winding number over $\mathbf{k}_\perp=(k_x,k_y)$[33,34]. Although the Majorana surface states can be gapped out by disorder which breaks translational symmetry locally, they will be restored after disorder averaging, similar to weak or crystalline topological insulators[35,36]. Interestingly, there exists a kind of disorder which can host Majorana modes locally. At a nematic vortex core, where three degenerate nematic domain walls meet, the Majorana Kramers pair return and pin to it[28].

V. DISCUSSION

The non-symmorphic crystal structure provides a proper electronic base for odd-parity pairing. Under time-reversal and inversion symmetries, the SOC is shown to favor equal-spin pairing and the E_{2u} state in which the triplet d vector is pinned to the x-y plane. This 2D representation state would then spontaneously break the rotation symmetry and produce a nematic order, as in $Cu_xBi_2Se_3$[19–21] which has being ultimately confirmed by nuclear magnetic resonance (NMR) experiments[19]. However, NMR measurement would fail to answer the direction of the d vector as in Sr_2RuO_4 because E_{2u} and A_u states are very close in energy (T_c difference being less than 5%) and external magnetic fields can easily unpin the d vector from the x-y plane. Therefore we suggest the proof can be realized in scanning tunneling spectroscopy or phase-sensitive measurements[41]. A salient point for this quasi-1D crystal is that it is a type-II superconductor with huge κ[24], thus forbidding vortex formation, so that pure Zeeman effect can be used to study transitions between superconducting states.

Recently, similar quasi-1D $\mathcal{A}_2Cr_3As_3$ ($\mathcal{A}$=K, Rb, Cs) superconductors with comparable T_c were reported[42–44], and suggested to be nodal unconventional superconductivity[44–47]. Although they share identical crystal structure as $\mathcal{M}_2Mo_6Se_6$, their different electron valences[48] lead to completely different Fermi surface structures, and consequently, distinct superconductivity theories. We also noted an unexpected superconductivity found in $Na_{2-x}Mo_6Se_6$ in which a large Na deficiency makes the localized system superconducting[49].

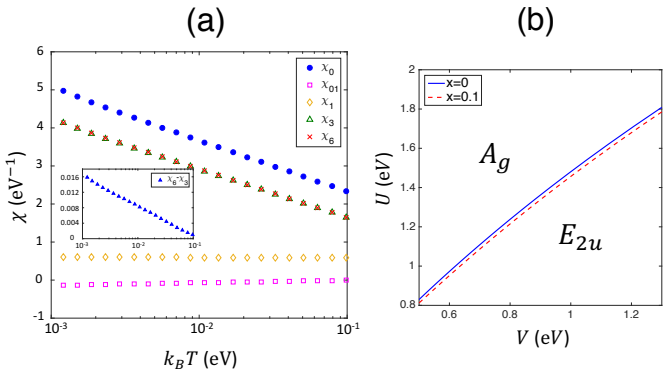

FIG. 3: (Color online) (a) Pair susceptibilities of $Tl_{2-x}Mo_6Se_6$ with $x = 0$ for relevant channels. Large χ_0, χ_3, and χ_6 correspond to A_g, A_u, and E_{2u} states, respectively. χ_3 and χ_6 curves almost overlap. (b) Superconducting phase diagram between A_g and E_{2u} states as functions of intra- and inter-sublattice interaction strengths, U and V. Doping has weak effect on the phase boundary. The range of V corresponds to T_c from about 10 K to 1000 K (nonlinear relation).

Acknowledgments

SMH was supported by the Ministry of Science and Technology (MoST) in Taiwan under grant No. 105-2112-M-110-014-MY3 and also by the NCTS of Taiwan. He also thanks S.-K. Yip for discussions and helpful suggestions. We would also like to thank Wei-Feng Tsai for a critical reading of the manuscript. The work at Northeastern University was supported by the US Department of Energy (DOE), Office of Science, Basic Energy Sciences grant number DE-FG02-07ER46352 (core research), and benefited from Northeastern University's Advanced Scientific Computation Center (ASCC), the NERSC supercomputing center through DOE grant number DE-AC02-05CH11231, and support (applications to layered materials) from the DOE EFRC: Center for the Computational Design of Functional Layered Materials (CCDM) under DE-SC0012575. H.L. acknowledges the Singapore National Research Foundation for the support under NRF Award No. NRF-NRFF2013-03.

Appendix A: Tight-binding model

We build up the low-energy Hamiltonian for $\mathcal{M}Mo_3Se_3$ according to symmetry. There are 12 symmetry elements in space group of $P6_3/m$ (No. 176). To derive the Hamiltonian, it suffices to use the inversion center ($\bar{1}$), the two-fold screw axis about z (2_1) and the three-fold rotation axis about z (3), since combinations of these three and their inverse elements can produce all possible operations. For example, the six-fold screw axis 6_3 corresponds to a three-fold rotation $\bar{3}$ followed by the two-fold screw 2_1. Two A and B sublattices in this nonsymmorphic crystal interchange under inversion and two-fold screw operations. Mathematically, the Hamiltonian follows

$$\mathcal{I}\mathcal{H}(k_x,k_y,k_z)\mathcal{I}^{-1} = \mathcal{H}(-k_x,-k_y,-k_z), \quad \text{(A1)}$$
$$\mathcal{S}_2\mathcal{H}(k_x,k_y,k_z)\mathcal{S}_2^{-1} = \mathcal{H}(-k_x,-k_y,k_z), \quad \text{(A2)}$$
$$\mathcal{C}_3\mathcal{H}(k_x,k_y,k_z)\mathcal{C}_3^{-1} = \mathcal{H}(k'_x,k'_y,k'_z), \quad \text{(A3)}$$

where $\mathcal{I}$, $\mathcal{S}_2$, and $\mathcal{C}_3$ stand for inversion, two-fold screw and three-fold rotation operators respectively. The momenta k''s in Eq. (A3) are given by

$$\begin{pmatrix} k'_x \\ k'_y \\ k'_z \end{pmatrix} = \begin{pmatrix} \cos\frac{2\pi}{3} & \sin\frac{2\pi}{3} & 0 \\ -\sin\frac{2\pi}{3} & \cos\frac{2\pi}{3} & 0 \\ 0 & 0 & 1 \end{pmatrix} \begin{pmatrix} k_x \\ k_y \\ k_z \end{pmatrix}. \quad \text{(A4)}$$

In addition, time-reversal symmetry for the physical system requires

$$\mathcal{T}\mathcal{H}(k_x,k_y,k_z)\mathcal{T}^{-1} = H(-k_x,-k_y,-k_z). \quad \text{(A5)}$$

1. Spinless case

We consider first the spinless two-band Hamiltonian, given by

$$\mathcal{H}_t(\mathbf{k}) = \sum_{i=0}^{3} \varepsilon_i(\mathbf{k})\sigma_i, \quad \text{(A6)}$$

where σ_0 and $(\sigma_1,\sigma_2,\sigma_3)$ are the identity and Pauli matrices in sublattice subspace. In this subspace, the symmetry operators are $\mathcal{I} = \sigma_1$, $\mathcal{S}_2 = e^{-ik_z/2}\sigma_1$, $\mathcal{C}_3 = \sigma_0$, and $\mathcal{T} = \sigma_0\mathcal{K}$. ($\mathcal{K}$ acting on ϕ gives the complex conjugate ϕ^*.)

Time-reversal symmetry (A5) imposes that $\varepsilon_2(\mathbf{k})$ must be odd in $\mathbf{k}$ and the other ε's even in $\mathbf{k}$. Inversion symmetry (A1) imposes that both $\varepsilon_2(\mathbf{k})$ and $\varepsilon_3(\mathbf{k})$ must be odd in $\mathbf{k}$. As a result, we have

$$\varepsilon_3(\mathbf{k}) = 0. \quad \text{(A7)}$$

Moreover, the two-fold screw symmetry (A2) imposes that $\varepsilon_2(\mathbf{k})$ must be odd in $\mathbf{k}_\perp = (k_x,k_y)$, i.e. $\varepsilon_2(-k_x,-k_y,k_z) = -\varepsilon_2(k_x,k_y,k_z)$, and $(\varepsilon_0(\mathbf{k}),\varepsilon_1(\mathbf{k}))$ even in $\mathbf{k}_\perp$. Combining the time-reveral symmetry and two-fold screw symmetry constraints on $\varepsilon_{i=0,1,2}$, we find that they are all even in k_z.

Moreover, three-fold symmetry (A3) requires that $\varepsilon_{i=0,1,2}$ are three-fold-rotation invariant. So, $\varepsilon_i(\mathbf{k})$ can be written as a product of $\mathbf{k}_\perp$ and k_z parts, namely $\sum_{j=1,2,3} f(\mathbf{k}_\perp\cdot\vec{\delta}_j)g(k_z)$. The Bravais vectors $(\vec{\delta}_1,\vec{\delta}_2,\vec{\delta}_3)$ are interchangeable under $\mathcal{C}_3$. As a result, we get

$$\begin{aligned}\varepsilon_0(\mathbf{k}) = {} & E_0 + 2t_{01}\cos(k_z) + 2t_{02}\cos(2k_z) \\ & + 2\,\mathrm{Re}\left[T_1(\mathbf{k}_\perp)\right]\left[t'_{00} + 2t'_{01}\cos(k_z) + 2t'_{02}\cos(2k_z)\right] \\ & + 2\,\mathrm{Re}\left[T_2(\mathbf{k}_\perp)\right]\left[t''_{00} + 2t''_{01}\cos(k_z) + 2t''_{02}\cos(2k_z)\right], \end{aligned} \quad \text{(A8)}$$

$$\begin{aligned}\varepsilon_1(\mathbf{k}) - i\varepsilon_2(\mathbf{k}) &= 2t_{11}\cos(k_z/2) + 2t_{22}\cos(3k_z/2) \\ &+ 2T_1(\mathbf{k}_\perp)\left[t'_{11}\cos(k_z/2) + t'_{12}\cos(3k_z/2)\right] \\ &+ 2T_1^*(\mathbf{k}_\perp)\left[t'_{13}\cos(k_z/2) + t'_{14}\cos(3k_z/2)\right] \\ &+ 2T_2(\mathbf{k}_\perp)\left[t''_{11}\cos(k_z/2) + t''_{12}\cos(3k_z/2)\right] \\ &+ 2T_2^*(\mathbf{k}_\perp)\left[t''_{13}\cos(k_z/2) + t''_{14}\cos(3k_z/2)\right],\end{aligned} \tag{A9}$$

where we consider finite hoppings up to second nearest neighbors in the $x-y$ plane and define

$$T_1(\mathbf{k}_\perp) \equiv \sum_{i=1,2,3} \exp(i\mathbf{k}_\perp \cdot \mathbf{a}_i), \tag{A10}$$

$$T_2(\mathbf{k}_\perp) \equiv \sum_{i=1,2,3} \exp\left[i\mathbf{k}_\perp \cdot (\mathbf{a}_{i+1} - \mathbf{a}_i)\right], \tag{A11}$$

with primitive vectors $\mathbf{a}_1 = \mathbf{a}_4 = (\frac{\sqrt{3}}{2}, -\frac{1}{2}, 0)$, $\mathbf{a}_2 = (0, 1, 0)$, and $\mathbf{a}_3 = (-\frac{\sqrt{3}}{2}, -\frac{1}{2}, 0)$. Equation (A9) is such that $\varepsilon_1(\mathbf{k}) = \varepsilon_2(\mathbf{k}) = 0$ at $k_z = \pi$, as required by the $\mathcal{TS}_2$ symmetry (see the main text).

2. Spinful case

Now, we introduce spin-orbit coupling. The spinful Hamiltonian then reads as $\mathcal{H}(\mathbf{k}) = \sum_{i,j=0}^{3} d_{ij}(\mathbf{k}) s_i \sigma_j$, where s_0 and (s_1, s_2, s_3) are the identity and Pauli matrices for spin. The symmetry operators from Eqs. (A1) to (A5) in spin-sublattice subspace are $\mathcal{I} = s_0\sigma_1$, $\mathcal{S}_2 = ie^{-ik_z/2} s_3\sigma_1$, $\mathcal{C}_3 = \sigma_0 e^{i\frac{\pi}{3}s_3}$, and $\mathcal{T} = is_2\sigma_0\mathcal{K}$.

The s_0 terms in the Hamiltonian immediately give $d_{0j}(\mathbf{k}) = \varepsilon_j(\mathbf{k})$. For those s_i terms with $i = (1, 2, 3)$, inversion symmetry (A1) gives

$$d_{ij}(-\mathbf{k}) = (-1)^{\delta_{j2}+\delta_{j3}} d_{ij}(\mathbf{k}), \tag{A12}$$

and time-reversal symmetry (A5) gives

$$d_{ij}(-\mathbf{k}) = (-1)^{\delta_{i1}+\delta_{i2}+\delta_{i3}} (-1)^{\delta_{j2}} d_{ij}(\mathbf{k}). \tag{A13}$$

So, they lead to

$$d_{i0}(\mathbf{k}) = d_{i1}(\mathbf{k}) = d_{i2}(\mathbf{k}) = 0, \tag{A14}$$

$$d_{i3}(-\mathbf{k}) = -d_{i3}(\mathbf{k}). \tag{A15}$$

Considering two-fold screw symmetry in Eq. (A2), we have for $i = 1, 2, 3$

$$d_{i3}(-k_x, -k_y, k_z) = (-1)^{\delta_{i3}} d_{i3}(k_x, k_y, k_z),$$

which imposes that $(d_{13}(\mathbf{k}), d_{23}(\mathbf{k}))$ are even in $\mathbf{k}_\perp$ and odd in k_z, while $d_{33}(\mathbf{k})$ is odd in $\mathbf{k}_\perp$ and even in k_z. Finally, the three-fold rotation symmetry (A3) imposes

$$d_{13}(\mathbf{k}') - id_{23}(\mathbf{k}') = e^{i\frac{2\pi}{3}} \left(d_{13}(\mathbf{k}) - id_{23}(\mathbf{k})\right), \tag{A16}$$

$$d_{33}(\mathbf{k}') = d_{33}(\mathbf{k}). \tag{A17}$$

We can use the rotation relations in Eq. (A4) to write down all possible forms for d_{i3}.

Let's define $\zeta_i(\mathbf{k}) = d_{i3}(\mathbf{k})$ $(i = 1, 2, 3)$. The full Hamiltonian reads

$$\mathcal{H}(\mathbf{k}) = s_0\mathcal{H}_t(\mathbf{k}) + \sum_{i=1,2,3} \zeta_i(\mathbf{k}) s_i\sigma_3, \tag{A18}$$

where $\mathcal{H}_t$ is given in Eq. (A6). Again by writing ζ_i as a product of $\mathbf{k}_\perp$ and k_z parts, we get

$$\begin{aligned}\zeta_1(\mathbf{k}) - i\zeta_2(\mathbf{k}) &= 4R_1(\mathbf{k}_\perp)\left[\lambda'_{11}\sin(k_z) + \lambda'_{12}\sin(2k_z)\right] \\ &+ 4R_2(\mathbf{k}_\perp)\left[\lambda''_{11}\sin(k_z) + \lambda''_{12}\sin(2k_z)\right],\end{aligned} \tag{A19}$$

$$\begin{aligned}\zeta_3(\mathbf{k}) &= 2\,\mathrm{Im}\left[T_1(\mathbf{k}_\perp)\right]\left[\lambda'_{00} + 2\lambda'_{01}\cos(k_z) + 2\lambda'_{02}\cos(2k_z)\right] \\ &+ 2\,\mathrm{Im}\left[T_2(\mathbf{k}_\perp)\right]\left[\lambda''_{00} + 2\lambda''_{01}\cos(k_z) + 2\lambda''_{02}\cos(2k_z)\right],\end{aligned} \tag{A20}$$

where in-plane functions $R_{1,2}$ are

$$R_1(\mathbf{k}_\perp) = \sum_{i=1,2,3} e^{-i\theta_i} \cos(\mathbf{k}_\perp \cdot \mathbf{a}_i), \tag{A21}$$

$$R_2(\mathbf{k}_\perp) = \sum_{i=1,2,3} e^{-i\theta'_i} \cos\left[\mathbf{k}_\perp \cdot (\mathbf{a}_{i+1} - \mathbf{a}_i)\right], \tag{A22}$$

where θ_i (θ'_i) is the angle of $\mathbf{a}_i$ ($\mathbf{a}_{i+1} - \mathbf{a}_i$) relative to the x axis. Table II lists the hopping and spin-orbit coupling parameters for our band fitting results for $Tl_2Mo_6Se_6$.

Appendix B: Estimate T_c difference between A_u and E_{2u} states

For the short-range interaction Hamiltonian

$$\begin{aligned}H_{\mathrm{int}} = -\sum_{\mathbf{r}} \Big\{ &U\left[n_{A\uparrow}(\mathbf{r})n_{A\downarrow}(\mathbf{r}) + n_{B\uparrow}(\mathbf{r})n_{B\downarrow}(\mathbf{r})\right] \\ &+ V\left[n_A(\mathbf{r})n_B(\mathbf{r} + \vec{c}/2) + n_A(\mathbf{r})n_B(\mathbf{r} - \vec{c}/2)\right]\Big\},\end{aligned} \tag{B1}$$

where $\mathbf{r}$ runs over the Bravais lattice and $n_X(\mathbf{r}) = n_{X\uparrow}(\mathbf{r}) + n_{X\downarrow}(\mathbf{r})$ is the electron density for sublattice X,

TABLE II: Hopping and spin-orbit coupling parameters in Eqs. (A8), (A9), (A19), (A20) of the tight-binding model for $Tl_2Mo_6Se_6$. All numbers are in units of eV.

E_0	t_{01}	t_{02}	t'_{00}	t'_{01}	t'_{02}	t''_{00}	t''_{01}	t''_{02}	
−0.1176	−0.0561	0.0023	−0.1041	−0.0449	−0.0023	0.0592	0.0365	0.0062	
t_{11}	t_{12}	t'_{11}	t'_{12}	t'_{13}	t'_{14}	t''_{11}	t''_{12}	t''_{13}	t''_{14}
1.0508	−0.0034	0.0901	0.0	−0.1203	0.0	−0.0271	0.0	0.0077	0.0
λ'_{00}	λ'_{01}	λ'_{02}	λ''_{00}	λ''_{01}	λ''_{02}	λ'_{11}	λ'_{12}	λ''_{11}	λ''_{12}
−0.0005	0.0015	−0.0005	−0.0001	−0.0001	−0.0002	0.0006	−0.0001	0.0	−0.0001

the possible order parameters are defined as follows

$$\begin{aligned}
A_g:\ \Delta_1 &= \frac{U}{4}\sum_{s=\pm(\uparrow\downarrow)} s\left\langle c^\dagger_{As}(\mathbf{r})c^\dagger_{A\bar{s}}(\mathbf{r}) + c^\dagger_{Bs}(\mathbf{r})c^\dagger_{B\bar{s}}(\mathbf{r})\right\rangle \\
&\quad + \frac{V}{2}\sum_{s=\pm} s\sum_{\eta=\pm}\left\langle c^\dagger_{As}(\mathbf{r})c^\dagger_{B\bar{s}}(\mathbf{r}+\eta\hat{c}/2)\right\rangle, \\
B_g:\ \Delta_2 &= \frac{V}{2}\sum_{s=\pm} s\sum_{\eta=\pm}\eta\left\langle c^\dagger_{As}(\mathbf{r})c^\dagger_{B\bar{s}}(\mathbf{r}+\eta\hat{c}/2)\right\rangle, \\
A_u:\ \Delta_3 &= \frac{V}{2}\sum_{s}\sum_{\eta=\pm}\eta\left\langle c^\dagger_{As}(\mathbf{r})c^\dagger_{B\bar{s}}(\mathbf{r}+\eta\hat{c}/2)\right\rangle, \\
B_u:\ \Delta_4 &= \frac{V}{2}\sum_{s}\sum_{\eta=\pm}\left\langle c^\dagger_{As}(\mathbf{r})c^\dagger_{B\bar{s}}(\mathbf{r}+\eta\hat{c}/2)\right\rangle, \\
E_{1u}:\ \Delta_5 &= \frac{V}{2}\sum_{s}\left\{\begin{array}{c} s \\ 1 \end{array}\right\}\sum_{\eta=\pm}\left\langle c^\dagger_{As}(\mathbf{r})c^\dagger_{Bs}(\mathbf{r}+\eta\hat{c}/2)\right\rangle, \\
E_{2u}:\ \Delta_6 &= \frac{V}{2}\sum_{s}\left\{\begin{array}{c} s \\ 1 \end{array}\right\}\sum_{\eta=\pm}\eta\left\langle c^\dagger_{As}(\mathbf{r})c^\dagger_{Bs}(\mathbf{r}+\eta\hat{c}/2)\right\rangle.
\end{aligned} \tag{B2}$$

The pair susceptibilities χ's are defined in the main text. Their numerical results are shown in Fig. 4, in which undoped ($x = 0$) and 5% hole doping ($x = 0.1$) are considered. No qualitative change in pairing susceptibilities by doping is observed. Three prominent channels χ_0, χ_3 and χ_6 correspond to A_g, A_u, and E_{2u} symmetries, respectively, all for sublattice-even pairing. Interestingly, the pairing susceptibilities for the A_u and E_{2u} channels are very close, as shown in the insets of Fig. 4. Pair susceptibilities for the gap functions in the form of $\cos(k_z/2)$, like B_u, are very weak since the normal-state Fermi surface is close to or even beyond the $k_z = \pi$ plane where gap functions vanish. Those for gapful superconductivity show the conventional logarithmic behavior, $\chi \sim \mathcal{N}_{\rm eff}\ln(\Lambda/k_{\rm B}T)$, where $\mathcal{N}_{\rm eff}$ stands for the weighted density of states and Λ is the energy cutoff.

To estimate the critical temperatures $T_{c,3}$ and $T_{c,6}$ for the A_u and E_{2u} channels, we shall adopt the simple BCS phenomenological formula,

$$\chi = \mathcal{N}_{\rm eff}\ln(\Lambda/k_{\rm B}T) \tag{B3}$$

to fit χ_3 and $(\chi_6 - \chi_3)$ calculated from the tight-binding model, as shown in Fig. 5. The resulting fitting parameters are given in Table III. A simple way to estimate their critical temperatures is to use

$$\begin{aligned}
k_{\rm B}T_{c,3} &= \Lambda\exp\left\{-\frac{1}{V\left(\mathcal{N}_{\rm eff,6}-\Delta\mathcal{N}_{\rm eff}\right)}\right\} \\
&\simeq \Lambda\exp\left\{-\frac{1}{V\mathcal{N}_{\rm eff,6}}\left(1+\frac{\Delta\mathcal{N}_{\rm eff}}{\mathcal{N}_{\rm eff,6}}\right)\right\} \\
&= \Lambda\left(\frac{k_{\rm B}T_{c,6}}{\Lambda}\right)^{\left(1+\frac{\Delta\mathcal{N}_{\rm eff}}{\mathcal{N}_{\rm eff,6}}\right)} = k_{\rm B}T_{c,6}\times\left(\frac{k_{\rm B}T_{c,6}}{\Lambda}\right)^{\frac{\Delta\mathcal{N}_{\rm eff}}{\mathcal{N}_{\rm eff,6}}}
\end{aligned} \tag{B4}$$

where we take $\Delta\mathcal{N}_{\rm eff} = \mathcal{N}_{\rm eff,6} - \mathcal{N}_{\rm eff,3} \ll \mathcal{N}_{\rm eff,6}$, and assume Λ is the same for both susceptibilities (but at fitting it is treated differently). By using the fitting parameters given in Table III, we can estimate the T_c difference for A_u and E_{2u} states. If we take $T_{c,6} = 6$ K, $T_{c,3}/T_{c,6} \simeq 0.95$ for $x = 0$ and $T_{c,3}/T_{c,6} \simeq 1$ for $x = 0.1$ in $Tl_{2-x}Mo_6Se_6$. So, within this doping range, the T_c difference is less than 5%.

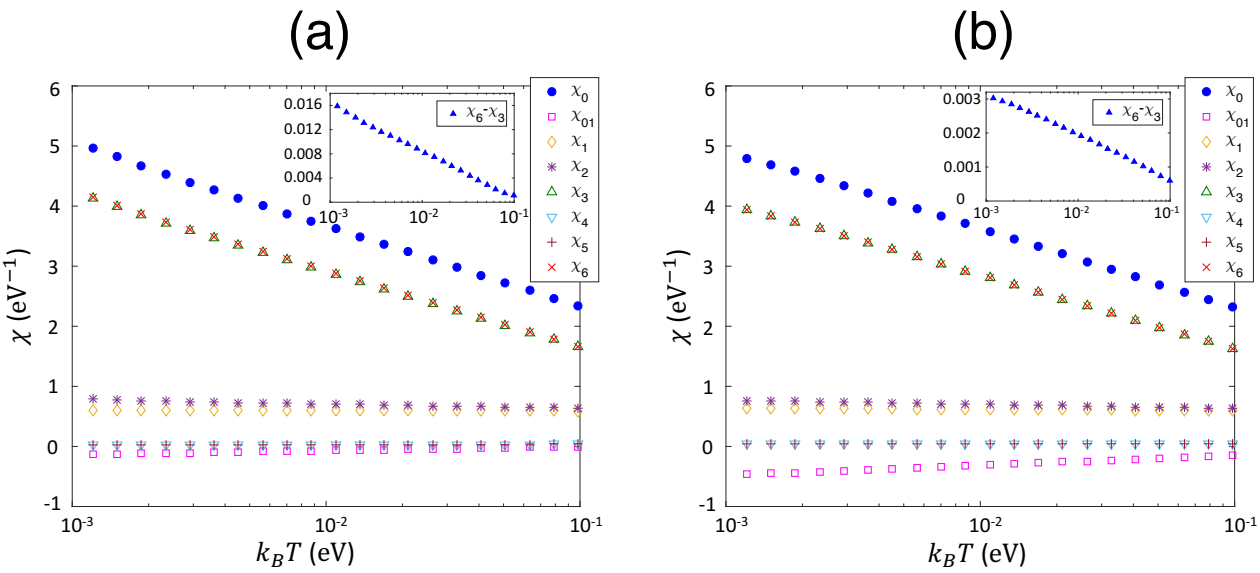

FIG. 4: (Color online) Pair susceptibilities of $Tl_{2-x}Mo_6Se_6$ for all channels for different dopings: (a) $x = 0$ ($\mu = 0$), and (b) $x = 0.1$ ($\mu = -0.176$ eV). The most dominant channel χ_0 corresponds to the A_g state, followed by χ_3 and χ_6 for A_u and E_{2u} states, respectively. Differences of χ_3 and χ_6 are shown in the insets.

TABLE III: Fitting parameters of χ_6 and χ_3 from Fig. 5.

x	$\mathcal{N}_{\mathrm{eff},6}^{\mathrm{fit}}$ (eV^{-1})	Λ^{fit} (eV)	$\Delta\mathcal{N}_{\mathrm{eff}}^{\mathrm{fit}}$ (eV^{-1})	$\Delta\chi_0^{\mathrm{fit}}$ (eV^{-1})
0	0.56	1.8352	0.0033	-0.0066
0.1	0.53	2.1270	0.00056	-0.00064

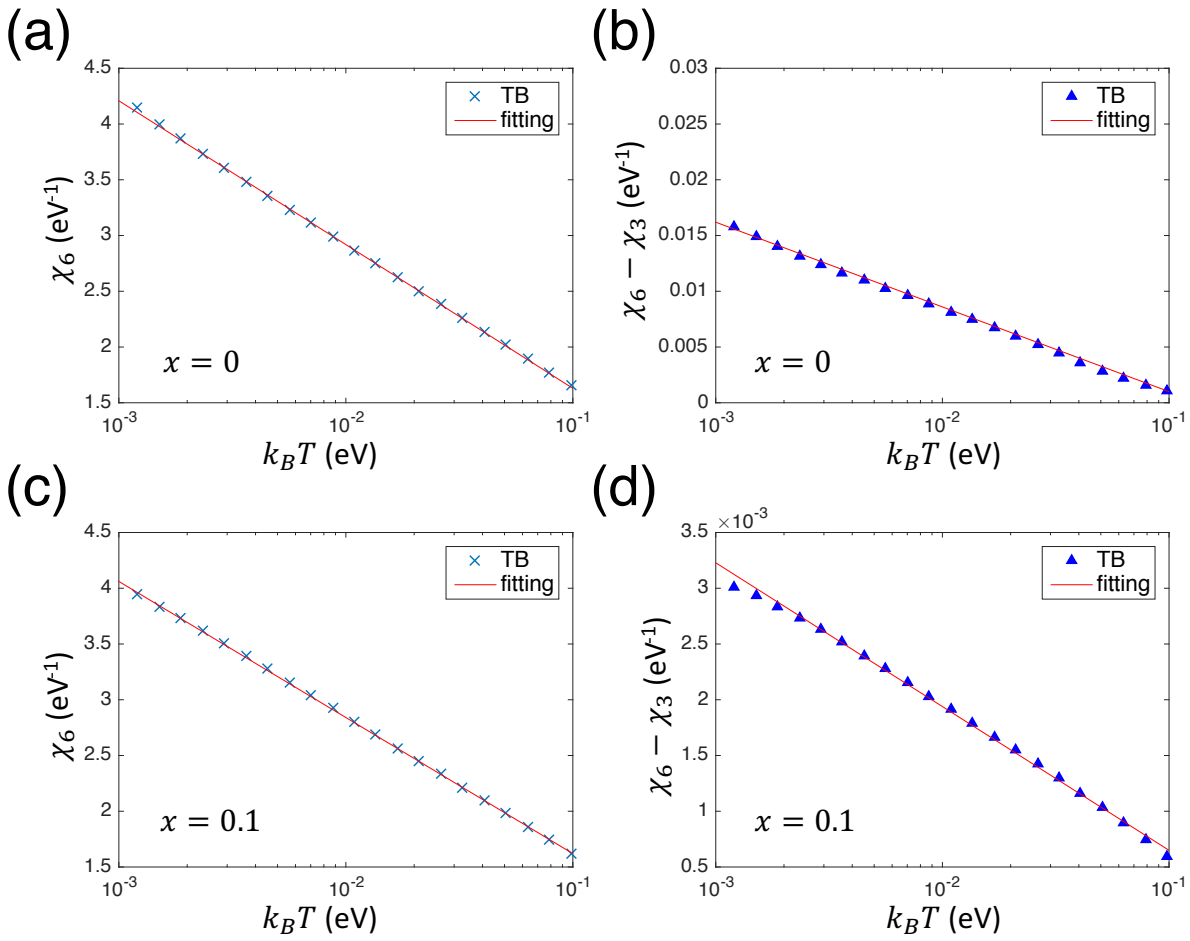

FIG. 5: (Color online) Fitting for χ_6 and $(\chi_6 - \chi_3)$ calculated from the tight-binding model (TB) for $x = 0$ (a,b) and $x = 0.1$ (c,d). The fitting formula for χ_6 is given by Eq. (B3), but the formula for $(\chi_6 - \chi_3)$ is given by $\Delta\chi_0^{\rm fit} - \Delta\mathcal{N}_{\rm eff}^{\rm fit} \ln(k_{\rm B}T)$. The resulting fitting parameters are given in Table III. We have chosen to fit the high temperature range above $k_{\rm B}T = 10^{-3}$ eV due to numerical limit.

[1] N. Read and D. Green, Phys. Rev. B **61**, 10267 (2000).
[2] D. A. Ivanov, Phys. Rev. Lett. **86**, 268 (2001).
[3] L. Fu and C. L. Kane, Phys. Rev. Lett. **100**, 096407 (2008).
[4] J. Alicea, Rep. Prog. Phys. **75**, 076501 (2012).
[5] M. Sato and S. Fujimoto, J. Phys. Soc. Jpn. **85**, 072001 (2016).
[6] M. Sato, Phys. Rev. B **81**, 220504(R) (2010).
[7] L. Fu and E. Berg, Phys. Rev. Lett. **105**, 097001 (2010).
[8] Y. Maeno, S. Kittaka, T. Nomura, S. Yonezawa, and K. Ishida, J. Phys. Soc. Jpn. **81**, 011009 (2012).
[9] M. W. Haverkort, I. S. Elfimov, L. H. Tjeng, G. A. Sawatzky, and A. Damascelli, Phys. Rev. Lett. **101**, 026406 (2008).
[10] J. A. Saul, Adv. in Phys. **43**, 113 (1994).
[11] J. Xia, Y. Maeno, P. T. Beyersdorf, M. M. Fejer, and A. Kapitulnik, Phys. Rev. Lett. **97**, 167002 (2006).
[12] E. R. Schemm, W. J. Gannon, C. M. Wishne, W. P. Halperin, and A. Kapitulnik, Science **345**, 190 (2014).
[13] J. D. Strand, D. J. Bahr, D. J. Van Harlingen, J. P. Davis, W. J. Gannon, and W. P. Halperin, Science **328**, 1368 (2010).
[14] E. Hassinger, P. Bourgeois-Hope, H. Taniguchi, S. René de Cotret, G. Grissonnanche, M. S. Anwar, Y. Maeno, N. Doiron-Leyraud, and Louis Taillefer, Phys. Rev. X **7**, 011032 (2017).
[15] Y. Oreg, G. Refael, and F. von Oppen, Phys. Rev. Lett. **105**, 177002 (2010).
[16] R. M. Lutchyn, J. D. Sau, and S. Das Sarma, Phys. Rev. Lett. **105**, 077001 (2010).
[17] S. Nadj-Perge, I. K. Drozdov, J. Li, H. Chen, S. Jeon, J. Seo, A. H. MacDonald, B. A. Bernevig, and A. Yazdani, Science **346**, 602 (2014).
[18] Y. S. Hor, A. J. Williams, J. G. Checkelsky, P. Roushan, J. Seo, Q. Xu, H. W. Zandbergen, A. Yazdani, N. P. Ong, and R. J. Cava, Phys. Rev. Lett. **104**, 057001 (2010).
[19] K. Matano, M. Kriener, K. Segawa, Y. Ando, and G.-q. Zheng, Nat. Phys. **12**, 852 (2016).
[20] L. Fu, Phys. Rev. B **90**, 100509(R) (2014).
[21] S. Yonezawa, K. Tajiri, S. Nakata, Y. Nagai, Z. Wang, K. Segawa, and Y. Maeno, Nat. Phys. **10**, 1038 (2016).
[22] J. Armici, M. Decroux, Ø. Fischer, M. Potel, R. Chevrel, and M. Sergent, Solid State Commun. **33**, 607 (1980).
[23] J. M. Tarascon, F. J. DiSalvo, and J. V. Waszczak, Solid State Commun. **52** 227 (1984).
[24] R. Brusetti, P. Monceau, M. Potel, P. Gougeon, and M. Sergent, Solid State Commun. **66**, 181 (1988).
[25] A. P. Petrović, R. Lortz, G. Santi, M. Decroux, H. Monnard, Ø. Fischer, L. Boeri, O. K. Andersen, J. Kortus, D. Salloum, P. Gougeon, and M. Potel, Phys. Rev. B **82**, 235128 (2010).
[26] B. Bergk, A. P. Petrović, Z. Wang, Y. Wang, D. Salloum, P. Gougeon, M. Potel, and R. Lortz, New J. Phys. **13**, 103018 (2011).
[27] A. P. Mackenzie and Y. Maeno, Physica B **280** 148 (2000).
[28] F. Wu and I. Martin, Phys. Rev. B **95**, 224503 (2017).
[29] P. Blaha *et al.*, WIEN2k, (Tech. Univ., Vienna, 2001).
[30] J. P. Perdew, K. Burke, and M. Ernzerhof, Phys. Rev. Lett. **77**, 3865 (1996).
[31] Q.-F. Liang, J. Zhou, R. Yu, Z. Wang, and H. Weng, Phys. Rev. B **93**, 085427 (2016).
[32] Q. Liu and A. Zunger, Phys. Rev. X **7**, 021019 (2017).
[33] M. Sato, Y. Tanaka, K. Yada, and T. Yokoyama, Phys. Rev. B **83**, 224511 (2011).
[34] A. P. Schnyder, P. M. R. Brydon, and C. Timm, Phys. Rev. B **85**, 024522 (2012).
[35] Y. Ando and L. Fu, Annu. Rev. Condens. Matter Phys. **6**, 361 (2015).
[36] Y. E. Kraus and A. Stern, New J. Phys. **13**, 105006 (2011).
[37] X. Dai, Z. Fang, Y. Zhou, and F. C. Zhang, Phys. Rev. Lett. **101**, 057008 (2008).
[38] P. M. R. Brydon, S. Das Sarma, H.-Y. Hui, and J. D. Sau, Phys. Rev. B **90**, 184512 (2014).
[39] P. A. Frigeri, D. F. Agterberg, A. Koga, and M. Sigrist, Phys. Rev. Lett. **92**, 097001 (2004).
[40] S.-K. Yip, Phys. Rev. B **87**, 104505 (2013).
[41] K. D. Nelson, Z. Q. Mao, Y. Maeno, and Y. Liu, Science **306**, 1151 (2004).
[42] J.-K. Bao, J.-Y. Liu, C.-W. Ma, Z.-H. Meng, Z.-T. Tang, Y.-L. Sun, H.-F. Zhai, H. Jiang, H. Bai, C.-M. Feng, Z.-A. Xu, and G.-H. Cao, Phys. Rev. X **5**, 011013 (2015).
[43] Z.-T. Tang, J.-K. Bao, Y. Liu, Y.-L. Sun, A. Ablimit, H.-F. Zhai, H. J., C.-M. Feng, Z.-A. Xu, and G.-H. Cao, Sci. China Mater. **58**, 16 (2015).
[44] Z.-T. Tang, J.-K. Bao, Y. Liu, Y.-L. Sun, A. Ablimit, H.-F. Zhai, H. Jiang, C.-M. Feng, Z.-A. Xu, and G.-H. Cao. Phys. Rev. B **91**, 020506 (2015).
[45] H. Z. Zhi, T. Imai, F. L. Ning, J.-K. Bao, and G.-H. Cao, Phys. Rev. Lett **114**, 147004 (2015).
[46] G. M. Pang, M. Smidman, W. B. Jiang, J. K. Bao, Z. F. Weng, Y. F. Wang, L. Jiao, J. L. Zhang, G. H. Cao, and H. Q. Yuan, Phys. Rev. B **91**, 220502(R) (2015).
[47] Y. Zhou, C. Cao, F. C. Zhang, Sci. Bull. **62**, 208 (2017).
[48] H. Jiang, G. Cao, and C. Cao, Sci. Rep. **5**, 16054 (2015).
[49] A. P. Petrović, D. Ansermet, D. Chernyshov M. Hoesch, D. Salloum, P. Gougeon, M. Potel, L. Boeri, and C. Panagopoulos, Nat. Commun. **7**, 12262 (2016).